A Study on Atmospheric Halo Visualization

Sung Min Hong and Gladimir Baranoski

Technical Report CS-2003-26

September, 2003

School of Computer Science
University of Waterloo
200 University venue West
Waterloo, Ontario, Canada N2L 3G1

Contents

List of Figures

Chapter 1

Introduction

Halos, arcs or spots of light in the sky, are caused by the play of sunlight on ice crystals in the atmosphere. In this project, a visualization model of the atmospheric halos is presented and demonstrated in the context of a Monte Carlo ray tracer. The model includes the geometric optics of hexagonal type crystals.

The impact of such simulations of natural phenomena has been to provide stunning confirmation of several extraordinary phenomena and extend our understanding of the nature. The deep understanding helps the improvement of many useful technology like the remote sensing of the atmosphere, then eventually improve our lives. In addition, increased computing power and plenty of measured atmospheric data have made it feasible to create physically correct halo images.

The structure of this report is outlined as follows. Chapter 2 explains what is the halo phenomena and what kind of halos exist. Chapter 3 gives brief descriptions of history, widely used ray tracing methods and current trends of the halo simulation. Chapter 4 presents a Monte Carlo ray tracer based on the idea of Pattloch and Tränkle [12]. The ray tracer uses a wavelength dependent refractive index for an ice crystal [3, 4]. Chapter 5 demonstrates some simulation results obtained by the method developed in chapter 4.

Chapter 2

Halo Phenomena

2.1 General description of halo phenomena

A halo is a luminous ring around the Sun or Moon. When it appears around the Sun, it is a solar halo; when it forms around the Moon, it is a lunar halo. Figure 2.1 shows various halo phenomena at the South Pole, which was taken by Tape [15]. Halos are produced all the year round from tropics to the poles by tiny ice crystals in cirrus clouds[1] 5 to 10km high in the always cold upper troposphere[2]. Sometimes in very cold weather they are also formed by crystals close to ground level. Ice crystals appear in front of buildings or other objects, and the association of halos with ice crystals becomes obvious.

The crystals behave like jewels, refracting and reflecting sunlight between their faces, sending light rays in particular directions. Regardless of their overall proportions, all the crystals have identical interfacial angles, which come from a deeper crystalline order at molecular scale. The submicroscopic order and symmetry give us regular and predictable halos. Walter Tape [15] collected the ice crystals when he took the picture, which is shown in figure 2.2.

Figure 2.2 shows the simple hexagonal shapes that produce a surprising variety of optical effects in the sky. The largest hexagonal crystal in that picture is about 0.5mm across, but typical dimensions of many of those crystals are 0.05 to 0.1mm [7]. When their ice crystals are smaller than 0.01mm, light is significantly diffracted, so halos are weak and diffuse. Crystals larger than 0.05mm refract and reflect light cleanly to produce halos. The sharpest halos occur when the crystals have precise alignments and this needs crystals larger than 0.1mm. However, the largest crystals of 1mm or more are rarely of sufficient optical quality and have defects which spoil their halos. These crystals are commonly aligned in particular directions. This results from the aerodynamic

[1] principal clouds type; a high elevation, wispy cloud without shadows.

[2] The troposphere is the lowest layer of Earth's atmosphere and site of all weather on Earth.

Figure 2.1: 22° halo at the South Pole redrawn from [15].

drag forces on crystals as they fall slowly downwards.

2.2 Ice crystal model and halo phenomena

Greenler [7] showed that all the halo phenomena results from reflecting from and refracting through the hexagonal ice crystal as they take on different shapes and orientations. The refraction halos show the partitioning of the incoming light into ice crystals due to the wavelength depended refraction leading to

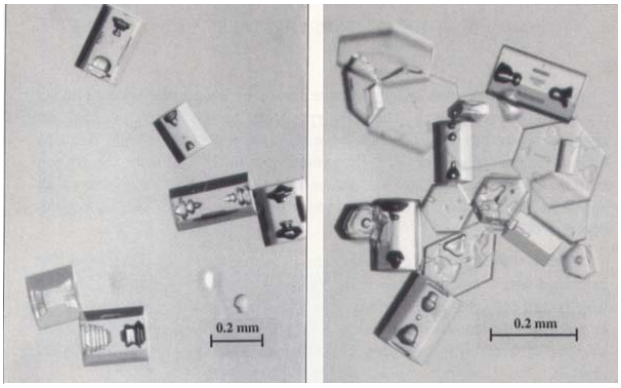

Figure 2.2: Some crystal collected at the South Pole redrawn from [15].

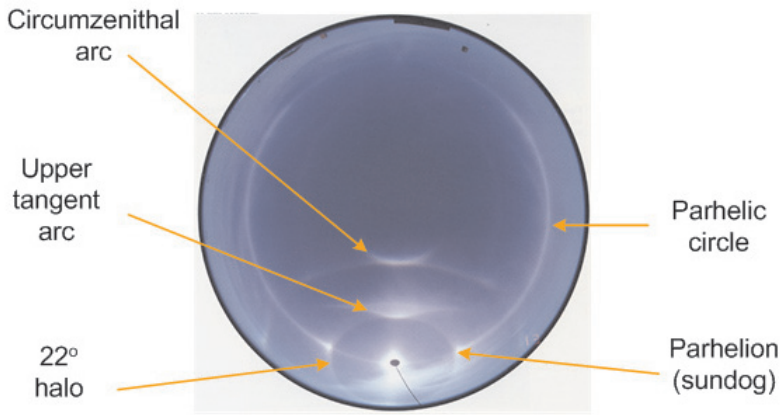

Figure 2.3: Frequent halos redrawn from [15].

colorful halos. These kinds of halos include 22° halo, parhelia (sundogs), circumzenithal halo and tangent arcs. On the other hand, the color of the reflection halos is unchanged leading to white, however when the sun is low in its elevation, the reflection halos caused by the sun become reddish. These latter halos include parhelic circle, pillar and so forth. Figure 2.3 shows how these halos can be seen in the sky.

A. Refraction halos

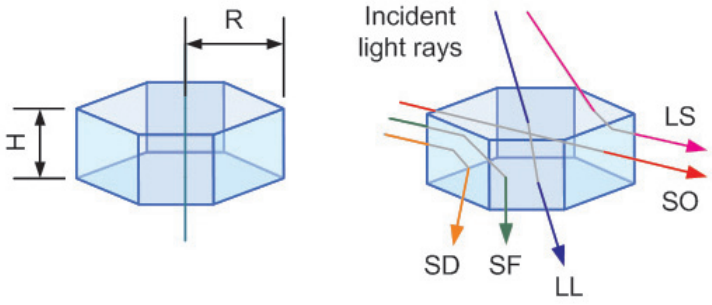

Figure 2.4: Ice crystal and light ray directions redrawn from [5]

Figure 2.4 shows a simplified simulation model for a hexagonal ice crystal. If the ratio of axial height to radius of its base is less than 2, the crystal is called a plate, otherwise called a pencil [7]. Greener [7] identified the sunlight

ray paths for various ice crystals and corresponding halos. Glassner [5] classified the paths of transmission paths through the crystal into five different types, which are illustrated in figure 2.4; "LL" for a path from a lid to another lid, "LS" for a path from a lid to a side face, "SD" for a path from a side to a directly adjacent side face, "SF" for a path from a side to a next side of a direct neighbor and "SO" for a path from a side to an opposite side. These light paths are reversible. Since the refraction coefficient of ice is approximately 1.31 and the neighboring side faces make 120° angle, there exist some important relationships between incident light and refracted light, which are responsible for the halo phenomena. Paths connecting neighbor sides, that is, "SD" can not occur in hexagonal type ice crystals because total internal reflection[3] occurs inside the crystals. "LL" and "SO" paths do not change light paths. The remaining light paths, "LS" and "SF" explain various halo phenomena; according to ice crystal facial orientation with respect to the incident rays, the rays will deflect them to a lesser or greater extent [7].

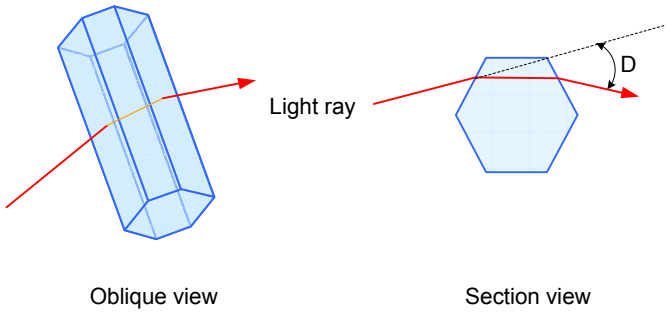

Figure 2.5: Mechanism of 22° halos redrawn from [7].

22° and 46° halos

22° halos are visible all over the world and throughout the year. Millions of ice crystals glint down from 3 to 5 mile high cirrostratus[4] haze to form a halo. figure 2.5 shows that the "SF" rays in figure 2.4 gives these halos. The rays pass randomly aligned hexagonal prism crystal with faces inclined at 60° to each other. The random orientations form a circular halo. Rays passing through two of their side faces are deflected through angles from 22° up to a

[3]For incident angles greater than or equal to a critical angle, all the incoming energy is reflected back into the incident medium.

[4]principal cloud type: a high elevation fibrous cloud of large extent without shadows.

little bit over 40°, which are expressed as "D" in figure 2.6. Skew rays, which are not in a plane perpendicular to the prism axis, are deflected even further [7].

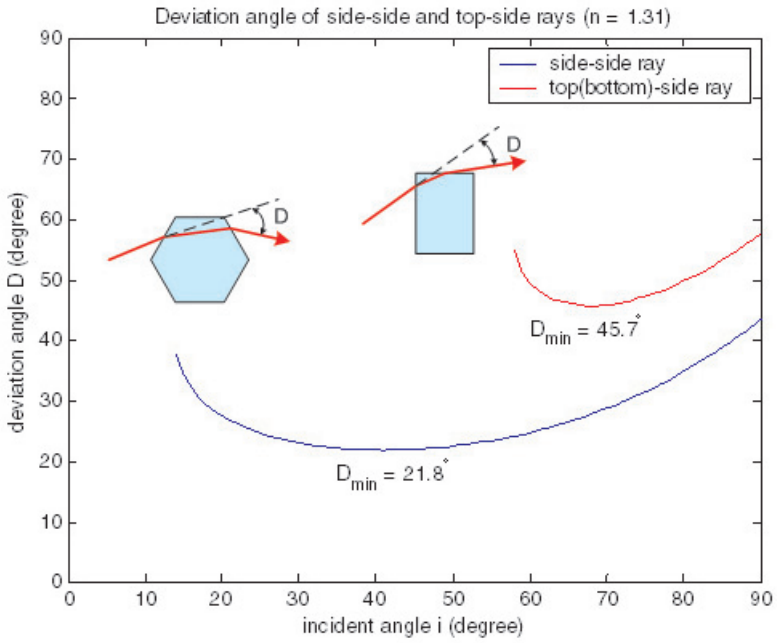

Figure 2.6: Deviation angles for 22° and 46° halos redrawn from [10].

Figure 2.6 shows why most rays, however, are deflected through angles close to 22°. This is the so-called "minimum deviation" phenomenon. The large plateau around the minimum deviation angle in figure 2.6 explaines that rays cluster together near to the angle where they are deviated least [7]. Near the minimum-deviation orientation, the deviation of the light ray is sensitive to small rotations of the crystal; that is, the direction of the emerging ray changes very little as the crystal is rotated several degrees either way from the minimum position. As a consequence, when light rays pass through crystals with all possible orientations, there is a concentration of rays deviated by angles near 22°. This gives 22° halos a bright inner edge. Rays deflected more than 22° produce the outer halo light which fades away with increasing angular distance from the Sun. Unlike 22° halos, light rays from top (bottom) to side or from side to top (bottom) are responsible for 46° halos. As shown in figure 2.6, the allowable incident angle range of 46° halos is much smaller than that of

22° halos, so the brightness of 46° halos is lower than that of 22° halos. This explains that 46° halos are frequently invisible while 22° halos are bright.

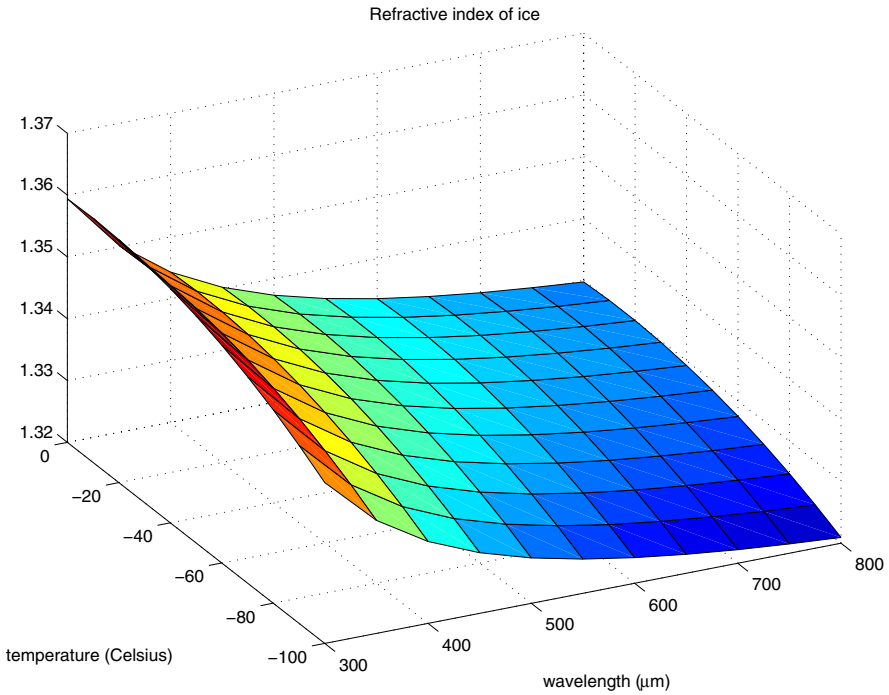

Figure 2.7: Refractive index vs. wavelength and temperature redrawn from [4].

Figure 2.7 shows the refractive index variation of ice as the wavelength of the incident light and the temperature change. Since the sunlight is composed of various wavelength components, every ice crystal plays a role of a prism for the sunlight. According to figure 2.7, red light component having long wavelength is refracted less strongly than other color components because the ice crystal has a smaller refractive index for long wavelength light than that for short wavelength components. Therefore, the halo's inner edge is red hued sometimes tapering away through oranges and yellows to blue. All but red are indistinct and washed out because they overlap considerably [11].

To see a ray of sunlight deviated by 22° directly to our eye, we would look at an angle 22° away from the Sun. The result of such refraction by a large number of ice crystals, tumbling through the air with random orientations, is a circle around the sun with the angular radius of the inner edge equal to 22°. Figure 2.8 shows the viewing mechanism of 22° halos and its photo by [7].

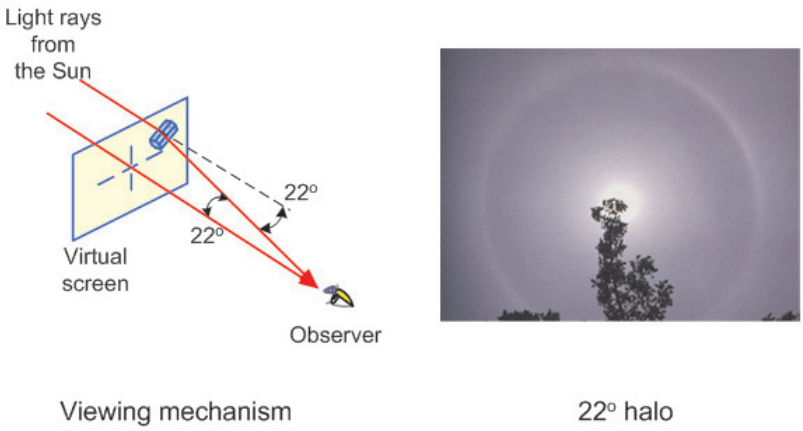

Figure 2.8: 22° halos and viewing mechanism redrawn from [7].

Parhelion (sundog)

Sundogs (parhelia, mock suns) are the second most frequent of the halos. Ice crystals do not always fall with random orientations. Plate crystals will tend to fall with the axis connecting its flat bases vertical, the flat bases oriented nearly horizontally. With the sun low in the sky, these plate crystals would have the proper orientation to refract light to the observer from the sides of the halo, but not from the top of the halo. The better the orientation of the ice crystals, the smaller and brighter are the resulting spots on either side of the sun. In some cases they can be quite bright and of an apparent size comparable to that of the sun. Parhelia are often brightly colored because the crystals refract each color by a different amount [7]. Figure 2.9 shows a typical light path in an ice crystal and a photo of sundog.

The colors most visible in halos are the longer wavelengths: red, orange, and yellow. There are three reasons for this [10]. First, dispersion[5] is least for these wavelengths and they are not spread over nearly as large an angle in the sky as the short wavelengths are. This makes them brighter than the short wavelengths, which is well explained in figure 2.6. Second, most halos are seen against the bluish background sky. The greens and blues blend in, leaving the reds and oranges showing the strongest color contrast. Third, when the sun is low in the sky, it usually appears yellow-orange in color due to Rayleigh scattering and absorption. The ice crystals receive more of the longer wavelength than the shorter ones, and scatter them accordingly.

For skew rays, the angle of minimum deviation is greater than for normal

[5]In this context, this refers to separation of sunlight into colors by refraction

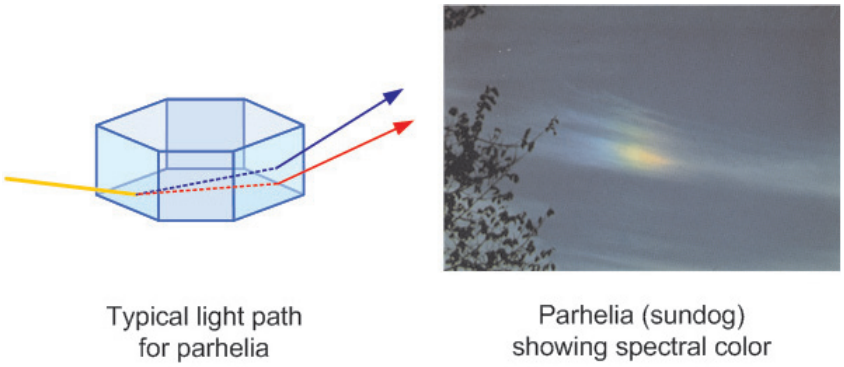

Figure 2.9: Light pass in ice crystal and parhelia photo redrawn from [7].

rays, and the angle increases as the skew increases. This effect is manifested in the distance of parhelia from the Sun for different elevations of the Sun. If falling plate crystals are oriented with their bases horizontal, light from the sun on the horizon will pass through their normal plane and produce parhelia with an inner edge 22° away from the Sun. But as the Sun's elevation increases, the ray pass through these oriented plate crystals with more and more skew, and the resulting parhelia appear farther and farther from the sun. The effect is large enough that the parhelia can easily be seen to lie outside the 22° halo for moderate sun elevation. The simulation result will explains this phenomenon in chapter 5.

Circumzenithal arc

Like parhelia, circumzenithal arc is generated by plate crystals. The circumzenithal arc is colored near the top. The arc appears about 25 days a year, with spectral colors which are sometimes well separated like a rainbow. As its name suggests, it lies on a circle centered at the zenith. Computer simulations show parhelia and a circumzenithal arc caused by plate crystals falling with roughly horizontal orientations [15]. Down-coming Sun's rays enter the uppermost horizontal face and leave through a vertical side face. The refraction of rays nearly parallel to faces inclined at 90° produces very pure in the context of wavelength and well separated prismatic colors. When the sun is higher than about 32.3°, the rays cannot leave the side face but are instead totally internally reflected. Figure 2.10 shows a typical light path in a crystal and the bright colors in the circumzenithal arc.

B. Reflection halos

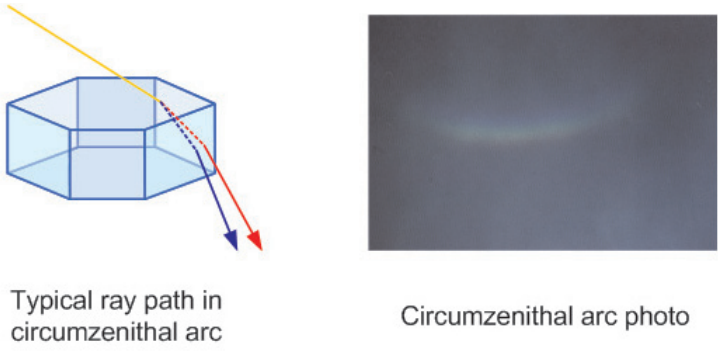

Figure 2.10: Light path for circumzenithal arc and photo redrawn from [7].

There is often a white band at sun's altitude, so white that it is sometimes easy to mistake it for cloud. This is the parhelic circle. When complete it goes all around the sky. Complete circles are rarities but sections extending outward from sundogs are quite common. It is formed by millions of ice crystals with vertical faces each mirroring the sun around the sky. This can be generated by externally reflected rays without rays entering the crystal or internally reflected rays. The simplest ray path is that of a single external reflection but there are many others, some most intricate. There can be no light color separation due to refraction, which is a kind of prism effect and so the arc is almost completely without color.

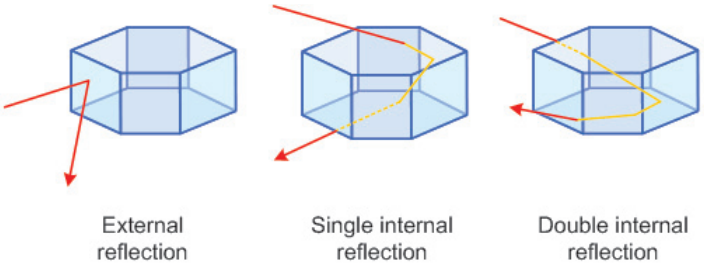

Figure 2.11: Typical light paths for parhelic circle redrawn from [15].

Figure 2.11 shows some reflection light paths responsible for the parhelic circle. External reflections contribute most near to the sun. Rays reflected once inside the crystals produce much of the halo intensity. Opposite the sun, rays internally reflected twice or even more add their brightness. Relative contributions depend on solar altitude and the crystal thickness.

A vertical mirror that intercepts a ray of light coming from the sun with

30° above the horizon reflects the light in a direction of 30° below the horizon. An observer would look up to see the ray coming from a direction of 30° above the horizon. As the vertical mirror addresses different directions around the horizon, it reflects the light in different azimuth directions, but always directs the light downward at an angle of 30° [7]. The result of a collection of vertical mirrors with all other possible orientations is a circle of white light extending around the sky at constant elevation above the horizon, passing thorough the sun. Figure 2.12 shows viewing mechanism and its photo [7, 15].

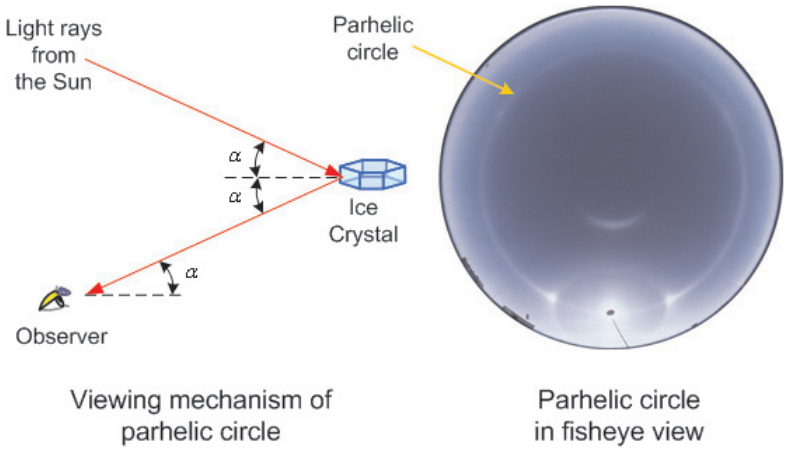

Figure 2.12: Viewing mechanism [7] and parhelic circle photo [15].

Chapter 3

Survey of Halo Simulation

3.1 History of halo simulation

For many halos, the orientations and ray paths have long been known, thanks to the ingenuity of many scientists over the past several centuries long before computers are used [15]. In the late 17th century, E. Mariotte showed how randomly oriented crystals would cause the 22° halo and how crystals with axes vertical would cause the parhelia(sundogs). In the mid-nineteenth M. A. Bravais described crystal orientations and ray paths for many common halos, and he calculated halo shapes as a function of sun elevation. In 1925, Wegener showed how to calculate the shapes of most of the known halos, illustrating his results with detailed plots of many infrequent halos. These earlier investigators used ray tracing methods with paper and pencil.

In 1980 Greenler [7] published his elegant *Rainbows, Halos, and Glories*. In his book, he explained how to apply a path tracing method to simulate halos with a computer. He got the intensity variations of simple halos and by superposing them, was able to describe complex halo phenomena. In 1984 Pattloch and Tränkle [12] introduced a hit and miss Monte Carlo method to display halos, which uses the Fresnel equations as reflection and transmission probabilities. With the method, they simulated infrequent halos, which can be explained by complex ice crystal displays. The impact of these simulations has been to provide stunning confirmation of several extraordinary halo displays and to resolve much of the controversy regarding the cause of the infrequent halos.

The early Monte Carlo simulation employed the assumption that each light beam strikes a perfectly formed crystal and then suffers no further scattering afterward. Tränkle and Greenler [16] included multiple scattering in clouds of finite optical depth to see if it could explain any unusual halo phenomena. Although they found that multiple scattering could account for a few rare phenomena such as parhelia with subparhelia, which mean several subsize

sundogs tailing the primary sundog, its primary effect is to wash out the halo beams. Takano and Liou [14] also considered multiple scattering effects on the visualization of halos. They computed halo phenomena caused by horizontally oriented plate and column ice crystals and showed the multiple scattering is responsible for some infrequent halos like an anthelion[1]. In addition to multiple scattering effects, Gedzelman [3] extends the computer simulations of halos by including color. He used an wavelength dependent index of refraction but excluded effects of polarization.

The proposed method mentioned above are mainly focused on the visualization as scientific purpose to identify what factors make halos and how the halos can be seen. Therefore, the final images of computer simulation are usually collections of coarse dots, which are good enough for verification purposes but far from realistic halo images. Glassner tried to overcome this gap, so he tried various blurring methods to transform dotted images into smooth images [5, 4]. Jackèl and Walter proposed an atmospheric rendering method in order to obtain realistic images in terms of Mie scattering and applied a parallel computation strategy for individual wavelength calculations [9]. And they put computer generated halo images into outdoor scenes which were also made by a computer. On the other hand, Gonzato and Marchand presented a technique for generating photo-realistic pictures of halos [6]. They indicated that Glassner's blurring method to obtain smooth halo images is not proper because it tries to apply an uniform reconstruction technique for a non-uniform sampling. Their method is based on an algorithm for reconstructing the uniform version of images from non-uniform samplings. With the technique, they obtained natural looking computer generated halos.

3.2 Basic Monte Carlo Methods

A. The Inverse Ray Tracing Algorithm

Greenler provided the physical foundation of almost all halo simulation algorithms [7]. He proposed to consider the case of a ray of sun being deviated by on single ice crystal during its travel through an ice cloud including the crystal. The problem is to compute the quantity of light passing through each pixel of the image representing the simulated halo. From the complexity point of view, using a standard ray tracing algorithm is not feasible. Indeed, for a ray leaving the eye and passing through the pixel, the algorithm has to test all the orientations in order to find the ones which deviate the ray into the direction of the light source. Greenler proposed to use an inverse ray tracing algorithm instead. Knowing the direction of the ray of light leaving the crystal is equivalent to knowing where to look in the sky for light coming to your eye

[1] A luminous white spot that appears on the parhelic circle and 180° in azimuth away from the sun.

from the crystal with that particular orientation. His algorithm is presented as the following 4 steps.

Step 1. Choose one crystal and select its orientation from possible random orientations

Step 2. Cast a ray from a light source like the sun to the crystal and calculate the deviation of ray.

Step 3. Place the crystal on a proper location in order to see the light ray from the light source. This positioning is simply done by plotting a light point on a fisheye view image of the atmosphere

Step 4. Repeat the previous steps for a preset number of light rays.

B. The Monte Carlo method

Pattloch and Tränkle defined a stochastic process for the reflection and refraction of the sunlight for a given distribution of crystals [12]. Paths of different ray classes occur, that is, whether the ray is reflected or transmitted is determined by the stochastic process. The algorithm follows the path for several internal reflections until it leaves the crystal. They repeated this numerical experiment for about 10^5 light rays and the number of repetitions seems to be sufficient for the intensity of all possible halos, but this number may not be enough for the visualization purpose because its output image is too crude. They explained a stochastic model with an ice crystal in figure 3.1, which is known to produce the 22° and 46° halos. The laws of geometrical optics at the first surface are given as

$$\alpha_1' = \alpha_1 \quad \text{(reflection law)} \tag{3.1}$$

$$\frac{\sin\alpha_1}{\sin\alpha_2} = n, \quad n \approx 1.31 \quad \text{(refraction law)}. \tag{3.2}$$

The Fresnel equations [8] for the reflection amplitudes for perpendicular, parallel polarization, and the reflectance in natural light are

$$r_\perp = -\frac{\sin(\alpha_1 - \alpha_2)}{\sin(\alpha_1 + \alpha_2)} \tag{3.3}$$

$$r_\parallel = \frac{\tan(\alpha_1 - \alpha_2)}{\tan(\alpha_1 + \alpha_2)} \tag{3.4}$$

$$R = \frac{1}{2}(r_\perp^2 + r_\parallel^2) \qquad \text{(see the appendix for details)}. \tag{3.5}$$

In the spirit of the hit-and-miss Monte Carlo method, the ray to be reflected or transmitted has the probability R or $1 - R$, respectively. In the case

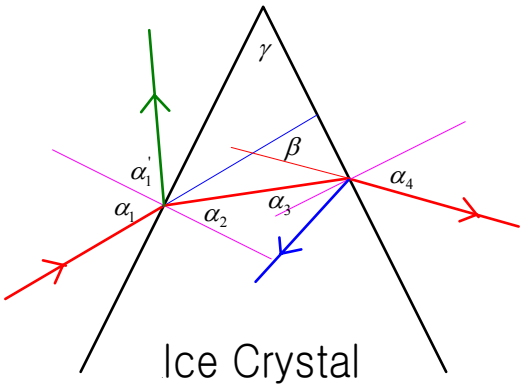

Figure 3.1: Typical paths of sunrays through an ice crystal

of transmission through the first surface, this procedure applied again at the second surface. The detail of their path algorithm is explained as follows and the 22° halo image obtained by this algorithm is shown in figure 3.2.

Step 1. Choose one crystal and select its orientation from possible random orientations.

Step 2. Cast a ray from a light source like the sun to the crystal.

Step 3. Decide whether the ray is reflected or transmitted. If it is reflected, plot a reflected ray along the direction of $\alpha_1' = 180° - 2\alpha_1$ and go to the next ray. If the ray is transmitted, determine the incident angle $\alpha_3 = \gamma - \alpha_2$ at second surface.

Step 4. If $n \sin \alpha_3 > 1$, the ray is totally reflected. Go on to the next ray. Otherwise, calculate α_1 and R^2 and decide if reflection or transmission occurs.

Step 5. If the ray is transmitted, plot a point along the direction $\beta = \alpha_1 + \alpha_4 - \alpha_2 - \alpha_3$. Go to Step 1.

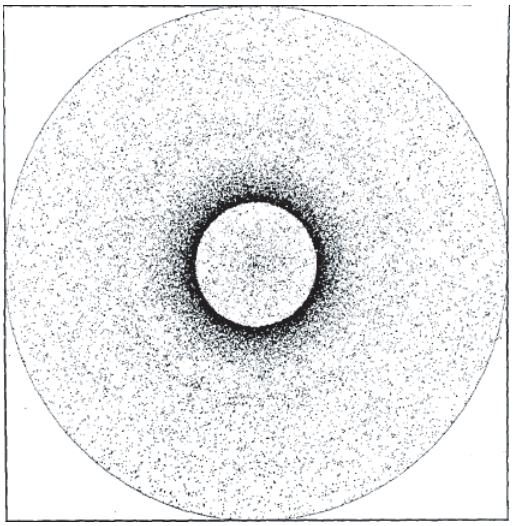

Figure 3.2: 22° halo image by the Monte Carlo ray tracing redrawn from [12]

3.3 Extended Monte Carlo Methods

A. Multiple Scattering Algorithm

When sunlight is scattered by a layer of ice crystals, some rays are scattered by two or more ice crystals in the layer, and some pass through without any scattering, which is shown in figure 3.3. Multiple scattering increases background intensity and the sharp structures of single scattering are smeared out [16]. In the region near the sun, multiple scattering effects of reflection and refraction may be superimposed upon diffraction effects. The multiple scattering effects are responsible for the 44° parhelion, the anthelion, and so forth.

The hit-and-miss Monte Carlo procedure used in single scattering is also appropriate to simulate multiple scattering of sunlight by a layer of ice crystals [16]. Takano and Liou[14] developed a radiative transfer method to solve the solar radiation in an optically anisotropic media like cirrus clouds including ice crystals. Using the radiative transfer schemes, they demonstrated scattering effects. They simulated halos produced by horizontally oriented ice crystals. Gedzelman extended his computer simulations of both halos and rainbows by using an algorithm to describe some of the effects of light scattering through the atmosphere and through clouds of finite optical thickness [3]. The following steps summarize the extended Monte Carlo method proposed by Tränkle and Greenler and a halo image by considering multiple scattering is shown in figure 3.4.

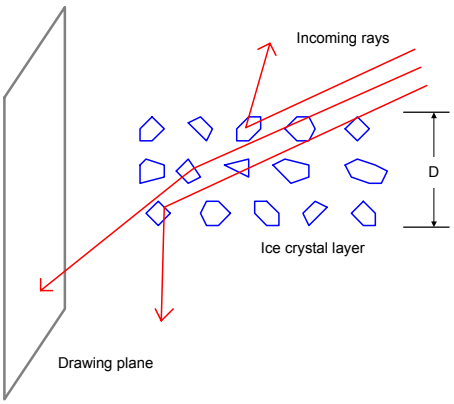

Figure 3.3: Model of ray tracing through ice crystal layer redrawn from [12]

Step 1. Follow the path of a ray from the Sun through a horizontal, plane-parallel layer of optical depth D in units of the mean free path. See figure 3.1. The incident angle is given by the sun elevation.

Step 2. Draw a random free path ℓ from the distribution $p(\ell) = \exp(-\ell)$ and new direction from the single scattering algorithm.

Step 3. Repeat the steps until the ray leaves the layer, above or below.

Step 4. Plot a point at the intersection of the ray with the drawing plane.

B. Coloring Halos

Gedzelman [3] used a wavelength dependent index of refraction in his simulation of halos and rainbows, which is $n_{\text{ice}} = 1.3203 - 0.0333\lambda\,(\mu m)$. It is not mentioned in [3] where he obtained the refractive index formula. Glassner [4] tried to obtain smooth color in halo images. The formula Glassner used for the index of refraction is derived from Sellmeier's formula, which is approximated in two term form, is $n_{\text{ice}} = A + \frac{B}{\lambda^2}$. The coefficient A and B are temperature dependent and shown as follows.

$$A(T) = 1.32491 - 0.00000399278T - 0.00000120678T^2, \tag{3.6}$$

$$B(T) = 3105.31 + 1.25203T - 0.0353608T^2, \tag{3.7}$$

where T is in Celsius. Figure 2.7 shows the refractive index variation according to the changes of wavelength and temperature.

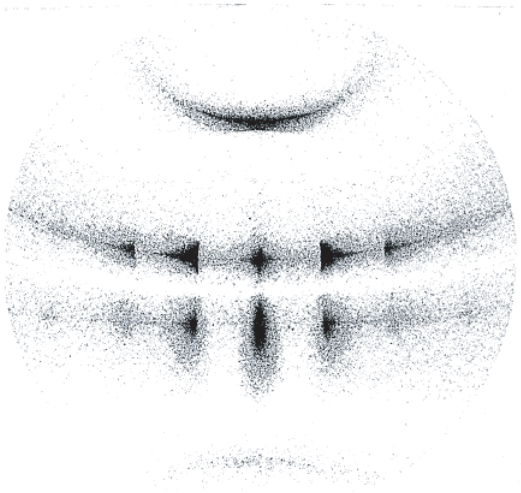

Figure 3.4: Complex halo image by multiple scattering redrawn from [16]

3.4 Photo Realistic Rendering

Glassner applied various smoothing methods to dot patterns existing in usual halo simulation images for naturally looking halo images [4]. His first trial is blurring the dotted image, then he applied a Gaussian blob over each spot and finally he used a multi-resolution composting method. The results of such trials were frequently too blurry or too speckled.

Jackèl and Walter [9] used a radiation intensity for the effects of scattering and absorption in rendering halos. They divided the atmosphere into cells to facilitate the visible radiation and assigned scattering and absorption parameters to each cell and calculated the scattered radiation pointing toward the observer. In their simulation, the scattering calculation for 21 different wavelengths were done to preserve dispersion effects. Each wavelength calculation was carried out by using parallel computing scheme. And they made the halo simulation as an integral parts of a virtual environment. Figure 3.5 shows one of their simulated images.

Gonzato and Marchand [6] addressed the problem Glassner mentioned, which is how to recover as accurately as possible as the missing data in halo simulation images in the Monte Carlo method. They indicated that Glassner tried to apply an uniform reconstruction technique for non-uniform sampling, so his method resulted in clumsy images. They proposed the irregular sampling

Figure 3.5: Computer generated 22° halo redrawn from [9]

theory for photo realistic[2] halo image reconstruction. They used the Marvasti-Allebach reconstruction algorithm [1] for picture issued from halo simulations. Their detail procedure is shown below and their halo image is shown in figure 3.6.

Step 1. Interpolate the unknown pixels by using the known sampling values. Many interpolation techniques can be used, such as the Voronoi interpolation: nearest neighborhood interpolation, using the arithmatic mean for equally-spaced neighbors.

Step 2. Apply a low pass filtering to the interpolated picture. Perform a local non-uniform reconstruction by adaptively choosing for every pixel the best size for reconstruction filter.

Step 3. Compare the reconstructed picture and the original one. If the error, which is the square sum of differences between original values and reconstructed values at known pixel points, exceeds a predetermined limit, then repeat the first two steps.

Glassner's [4] trial to smooth colors in halo images and transform the raw images into visually realistic halo images, seems to be unsuccessful, which is

[2]In this context, it means that computer generated halos look as if they had been natural scenes captured by a camera.

Figure 3.6: Computer generated halo in outdoor scene redrawn from [6]

mentioned in the beginning of this section. Jackèl and Walter [9] assert that their method can give realistic looking halo images by using atmospheric rendering technique and various wavelength rays, but they didn't mention anything about postprocessing[3] after obtaining ray-traced halo images. According to Gonzato and Marchand [6], the halo images obtained by the inverse ray tracing method have an intrinsic problem, that is, the pixels in the images are not uniformly sampled, so classic filtering methods based on regular sampling can not be applied to the halo images by satisfaction. They proposed a filtering method based on non-regular sampling and assert that their method can give photo realistic halo images without losing physical characteristics.

[3]In this context, postprocessing means interpolating and filtering of raw ray-traced halo images, which are proposed by Gonzato and Marchand [6]

Chapter 4

Implementation

The implementation of atmospheric halo visualization is composed of four sub parts. The first thing is to model an ice crystal using geometric parameters. Then it is necessary to define parameters for sun rays to reach observers via the ice crystal. The next thing is the parametrization of the ice crystal orientation, which enables us to adjust the crystal orientation according to the corresponding probabilities. Finally, the Monte Carlo ray tracing method is briefly described. As mentioned in the previous chapter, it is called an inverse ray tracing because it uses rays from the Sun instead of from the observer's eye.

4.1 Ice crystal modelling

There are many possible types of ice crystals. Laboratory experiments show that crystal type depends on the temperature and humidity under which the crystal forms and grows [15]. In cirrus clouds, ice tends to form simpler plates or columns which are shaped like pencils, under the appropriate combination of temperature and humidity. These hexagonal crystal forms produce a surprising variety of optical effects in the sky. In this work only this simple hexagonal shape will be considered because the crystal type can explain most halos and help us to understand the other halo phenomena. All the hexagonal forms are parameterized by two shape variables, which are shown in figure 4.1. The crystal is composed of eight polygons, which are used to check if the sunlight intersects the crystal. As mentioned earlier, when the sunlight hits the face of the crystal, it reflects or refract at the face depending upon the incident angle of the sunlight and the refractive index of the crystal. Sellmeier's formula for the refractive index of ice which was used by Glassner [4], is used in this work.

The orientation of ice crystal are described with Euler angles [2]. According to Euler's theorem, any rotations are defined by three parameters. Although there are several different notational conventions, in this work x-convention is

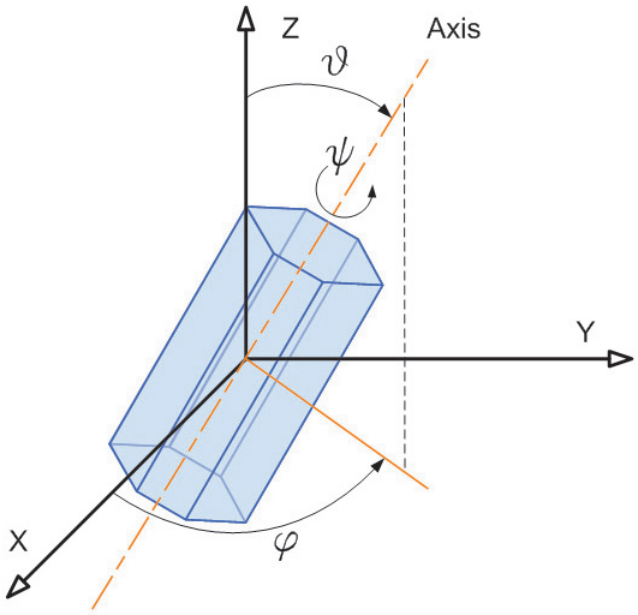

Figure 4.1: Parametric model of ice crystal

used. In the x-convention, the rotation given by Euler angles (ϕ, θ and ψ), where the first rotation is by an angle ϕ about the z-axis, the second is by an angle θ about the x-axis, and the third is by an angle ψ about the z-axis again.

4.2 Sunlight modelling

Since the Sun is far from the earth and the size of the Sun is much larger than that of the earth, the sunlight can be regarded as a set of collimated rays. The Sun is assumed to move only in y-z plane shown figure 4.2, so the rays from the Sun are parallel to the plane. Although the Sun is modelled as a point in y-z plane, all the rays for simulating the sunlight have different origins and same directions. The destinations of the rays are limited to the circle which is perpendicular to the rays. The radius of the circle should be large enough to include an entire ice crystal. The radius of the ray circle R can be given

$$R = \sqrt{r^2 + h^2} \tag{4.1}$$

The destination points of the rays are randomly determined. Let's two random variables be ξ_1 and ξ_2, respectively. Then the destination point of the

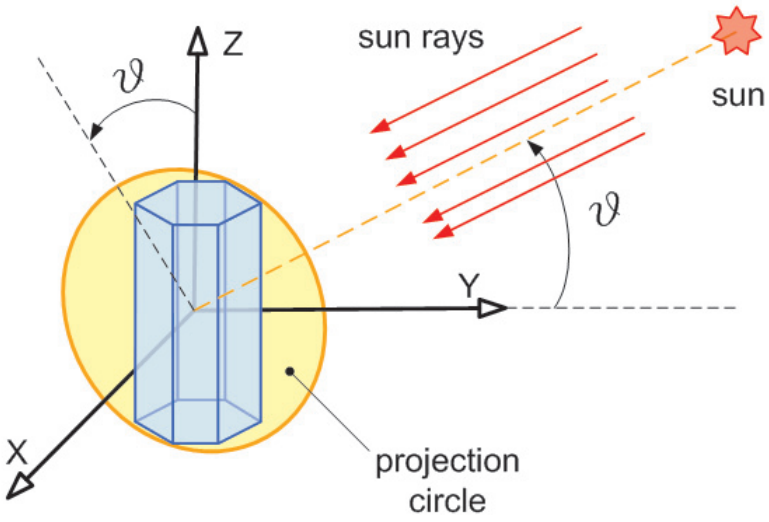

Figure 4.2: Sunlight model and projection circle

ray in the circle is represented by a azimuth angle ϕ and a radius ζ.

$$\phi = 2\pi\xi_1 \tag{4.2}$$

$$\zeta = R\cos^{-1}\left(\sqrt{1-\xi_2}\right) \tag{4.3}$$

And assuming that the elevation angle of the Sun is θ_{sun} and the distance from the center of the circle to the Sun is d, then a ray γ is defined as follows.

$$\gamma_{origin} = \{\zeta\cos\phi,\ d\cos\theta_{sun} - \zeta\sin\phi\sin\theta_{sun},\ d\sin\theta_{sun} + \zeta\sin\phi\cos\theta_{sun}\} \tag{4.4}$$

$$\gamma_{direction} = \{0,\quad -\cos\theta_{sun},\quad -\sin\theta_{sun}\} \tag{4.5}$$

4.3 Parametrization of ice crystal orientation

Pattloch and Tränkle [12] proposed probabilistic formula for the Euler angles of the ice crystal. According to them, the angular motion of the ice crystal in terms of the Euler angles can be described with crystal shape dependent probability formula. Since the angular motion of the crystal is stimulated by Brownian motion and atmospheric fluctuations, such nondeterministic expressions are more appropriate than deterministic expression. They classified the

ice crystals into 4 categories in order to give probabilistic expressions for the Euler angles.

(1) Randomly oriented tiny crystal or cubelike crystals; for the tiny crystals, a is not restricted, but $a \approx 1$ for the cubelike crystals.

$$p(\theta) = \frac{sin(\theta)}{2}, \qquad 0 \leq \theta < 180 \tag{4.6}$$

$$p(\phi) = \frac{1}{360}, \qquad 0 \leq \phi < 360, \tag{4.7}$$

$$p(\psi) = \frac{1}{360}, \qquad 0 \leq \psi < 360. \tag{4.8}$$

(2) Oriented plates with $a < 1$.

$$p(\theta) = \frac{1}{\pi} \frac{1}{\sqrt{\theta_m^2 - \theta^2}}, \qquad -\theta_m \leq \theta \leq \theta_m, \tag{4.9}$$

where $\theta_m = 0.4, -1.0$ or 2.5 in degrees, $p(\phi)$ and $p(\psi)$ are same as in (1).

(3) Singly oriented columns with $a > 1$. The same distribution functions are applied to these crystals, but the perfect orientation of θ is $\frac{\pi}{2}$.

(4) Doubly oriented columns with $a > 1$. In addition to θ, the perfect orientation of ϕ is set to 0. Because of the hexagonal symmetry of the crystal, there is an upper limit of the largest maximum rotation angle to ϕ, which is given $30°$.

$$p(\phi) = \frac{1}{60}, \qquad -30 \leq \phi \leq 30, \tag{4.10}$$

These mathematical expressions for the angular motion are very useful compared to the data for the angular motion given by Tape [15] because the former form is more convenient for simulation. However, the probabilistic forms are not so easy to be used in actual programs, so the mathematical expressions for the probabilities are converted into the direct expressions for θ, ϕ and ψ using three random variables ξ_1, ξ_2 and ξ_3. This function inversion procedure is mentioned in [13].

(1a) Randomly oriented crystals.

$$\theta = \arccos(1 - 2\xi_1), \qquad 0 \leq \xi_1 < 1 \tag{4.11}$$

$$\phi = 2\pi\xi_2, \qquad 0 \leq \xi_2 < 1, \tag{4.12}$$

$$\psi = 2\pi\xi_3, \qquad 0 \leq \xi_3 < 1. \tag{4.13}$$

(2a) Oriented plates with $a < 1$.

$$\theta = \theta_m \sin \pi(\xi_1 - 0.5), \qquad 0 \leq \xi_1 < 1, \tag{4.14}$$

where θ_m is same as given in (1) but in radians.

(3a) Singly oriented columns with $a > 1$.

$$\theta = \frac{\pi}{2} + \theta_m \sin \pi(\xi_1 - 0.5), \qquad 0 \leq \xi_1 < 1, \tag{4.15}$$

where ϕ and ψ are same as in (1a).

(4a) Doubly oriented columns with $a > 1$.

$$\phi = \pi + \frac{\pi}{6}(\xi_2 - 0.5), \qquad 0 \leq \xi_2 < 1. \tag{4.16}$$

4.4 Monte Carlo ray tracing

As mentioned in chapter 3, Greenler [7] introduced the computer aided simulation of the atmospheric halos. Pattloch and Tränkle extended his method by adopting Monte Carlo simulation. Afterwards, many researchers [16, 14, 3, 15, 5, 4, 9, 6] diversified their method by including the effects of multiple scattering, the wavelength dependency of the sunlight refraction, the complex shapes the crystals and etc. The Monte Carlo simulation used in this work is based on the method Pattloch and Tränkle [12] proposed in 1984. The simulation method is described as follows.

Preprocessing As mentioned in the previous sections 4.1 and 4.2, An ice crystal is modelled by 8 polygons, of which top and bottom polygons are hexagonal and sides are rectangular. The length of the hexagonal is set to 1 and the height of the rectangle is determined by the aspect ratio which varies according to the type of the ice crystal. The orientation of the crystal is determined by the Euler angles which are determined by three random variables ξ_1, ξ_2 and ξ_3.

Step 1. Set the following numbers before starting the ray tracing.
(a) Total number of rays to be traced.
(b) Elevation angle of the Sun.
(c) Proportions of ice crystals with different shape and orientation.
(d) Three different wavelength numbers(for example, red, green and blue[1]).
(e) Proportions of rays with different wavelength.

[1]These three colors are minimum number of colors to express a genral color and the number of colors can be increased in the actual programs.

Step 2. Randomly determine the following parameters whenever a new ray is created.
(a) The type of the ice crystal (for example, oriented plate with $a < 1$).
(b) The orientation of the ice crystal, θ, ϕ and ψ.
(c) The destination point of the ray in the projection circle.
(d) The wavelength of the ray.

Step 3. Check if the ray hits the crystal. If the ray misses the crystal, then increment the number of rays traced and go to Step 2.

Step 4. By using the wavelength dependent refractive index, which is shown figure 2.7 and explained in section 3.3, and the incident angle of the ray to the crystal, examine whether the ray refracts or reflects when the ray hit the crystal face. This step is briefly mentioned in the previous chapter 3.

Step 5. Trace the refracted ray or the reflected ray until it gets out of the crystal. The number of internal reflections is limited to 10, therefore when the number of the internal reflections exceeds this limit, then increment the number of rays and go to step 2.

Step 6. Check if the outgoing ray is visible to the observer. That is, if the crystal can be located on the upper hemisphere to give the same ray direction, we can decide whether the outgoing ray is visible or not.

Step 7. Add the ray color intensity to the pixel where the crystal should be located if the ray is visible.

Step 8. Increment the number of rays if the total number does not exceed the preset limit of the total ray numbers and go to Step 2. Otherwise, stop this simulation.

Chapter 5

Application

5.1 Initial setup

Before starting the simulation of various halos using the ray tracer developed in the previous chapter, several parameters without having random characteristics should be determined. As mentioned earlier, 4 different types of hexagonal ice crystals are used in this work. The proportions of the types should be determined before the simulation. The similar quantities are the sunlight color components, red, green and blue. The proportions of the color components in the sunlight and the corresponding wavelength are determined in advance. The aspect ratio of each crystal type varies every crystal by crystal, but the ratio for each crystal type is assumed to be fixed. The following shows the detail initial setup.

(1) Ice crystal data[1]

type	proportions	aspect ratio
randomly oriented	0.65	1.0
oriented plate	0.05	0.5
singly oriented	0.20	2.0
doubly oriented	0.10	2.0

(2) Sunlight color data[2]

[1] In the table, the proportions show a tentative set of composition and the aspect ratios are typical values.

[2] In the table, the proportions of red, green and blue show a tentative set of composition and the wavelengths for the colors are typical values.

color	proportions	wavelength (μm)
red	0.4	706
green	0.5	589
blue	0.1	404

In the above setup, the proportions of the crystal types vary according to the halo type. In the simulation, a ray contributes its corresponding color to a bluish background, where the color of the ray is determined randomly during the simulation. The background color is $(0.3, 0.3, 0.8)$. The red, green and blue contributions to the background are $(0.25, 0.0, 0.0), (0.0, 0.25, 0.0)$ and $(0.0, 0.0, 0.25)$, respectively. Besides, the sun elevation angle, the total number of rays, the limit of internal reflection and etc. are initially given.

5.2 22° halo simulation

In this simulation, the proportions of ice crystal types are $(1.0, 0.0, 0.0, 0.0)$. That is, there are only randomly oriented crystals floating in the air. The

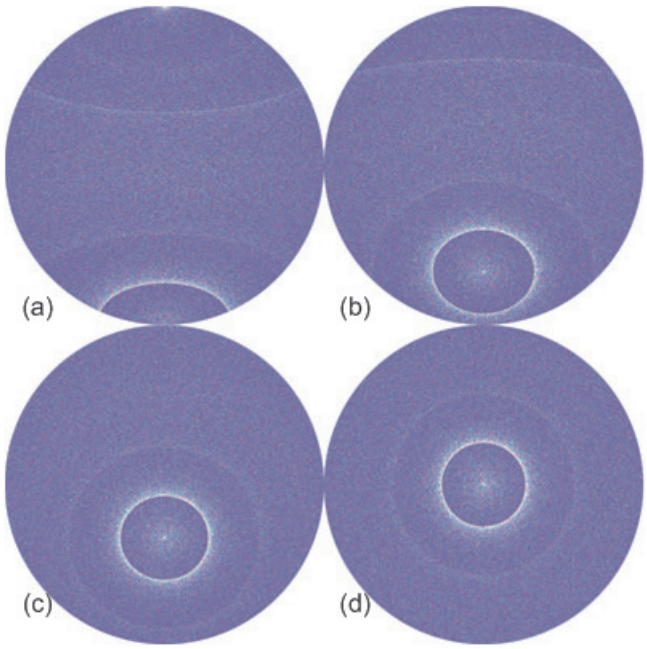

Figure 5.1: 22° halo vs. the Sun's elevation (a) 0° (b) 30° (c) 60° (d) 90°

total number of rays[3] is 2×10^6. These crystals causes a bright 22° degree halo and a faint 46° halo. These halos are positioned around the Sun, so the halos move with the Sun. Figure 5.1 shows the 22° and 46° around the Sun at different the Sun's elevations.

5.3 Parhelion and parhelic circle simulation

In this simulation, the proportions of ice crystal types are $(0.9, 0.1, 0.0, 0.0)$. There are majority of randomly oriented crystals and small portion of oriented plates floating in the air. The total number of rays is 2×10^6 as same as before. These crystals causes a bright 22° degree halo, a faint 46° halo, parhelia (sundogs) and parhelic circle. Figure 5.1 shows the halos around the Sun at different the Sun's elevations. As mentioned in chapter 2, the sundogs move away from the 22° halo circle as the Sun's elevation angle increase. In addition to the sundogs (the parhelia close to the Sun), the simulation shows 120° parhelia.

5.4 Composite halo simulation

In this composite halo simulation, the proportions of ice crystal types are $(0.65, 0.05, 0.20, 0.10)$. There are still majority of randomly oriented crystals, small portion of oriented plates, significant portions of singly and doubly oriented crystals floating in the air. The total number of rays is 3×10^6, which is increased from 2×10^6 to show various kinds of halos. These crystals causes a upper tangent arc, a supralateral and more in addition to the halos mentioned above. Figure 5.3 shows the simulated halos with the photo taken at the South Pole by W. Tape [15]. According to Tape [15], singly oriented columns cause the tangent arcs, supralateral arcs and some parhelic circle intensity. It is noticeable that there are a lot of similarities between the simulation image and the photo.

Figure 5.4 shows the frontal viewing images obtained with 90° horizontal and vertical viewing angles unlike the above fisheye viewing images. The simulation image closes up the upper tangent arc and the parhelia (sundogs). The figure also compares the picture taken by W. Tape [15]. The simulation describes the real halo image very closely. This simulation is obtained when the Sun is at 20° in its elevation angle. To obtain this image, 10^7 rays, which is needed to give proper intensities of halo images in the frontal view, are used.

[3]The number of rays is selected to give proper intensities to halo images.

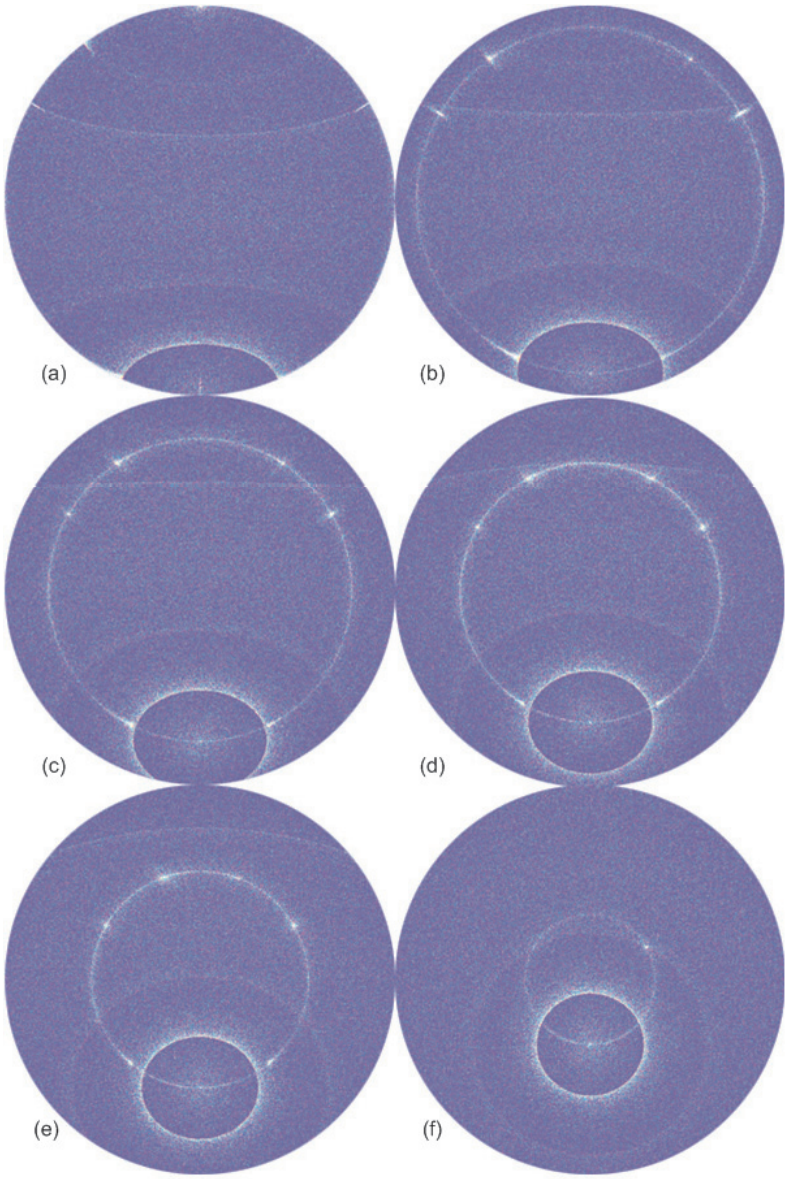

Figure 5.2: Parhelia vs. the Sun's elevation (a) 0° (b) 10° (c) 20° (d) 30° (e) 40° (f) 50°

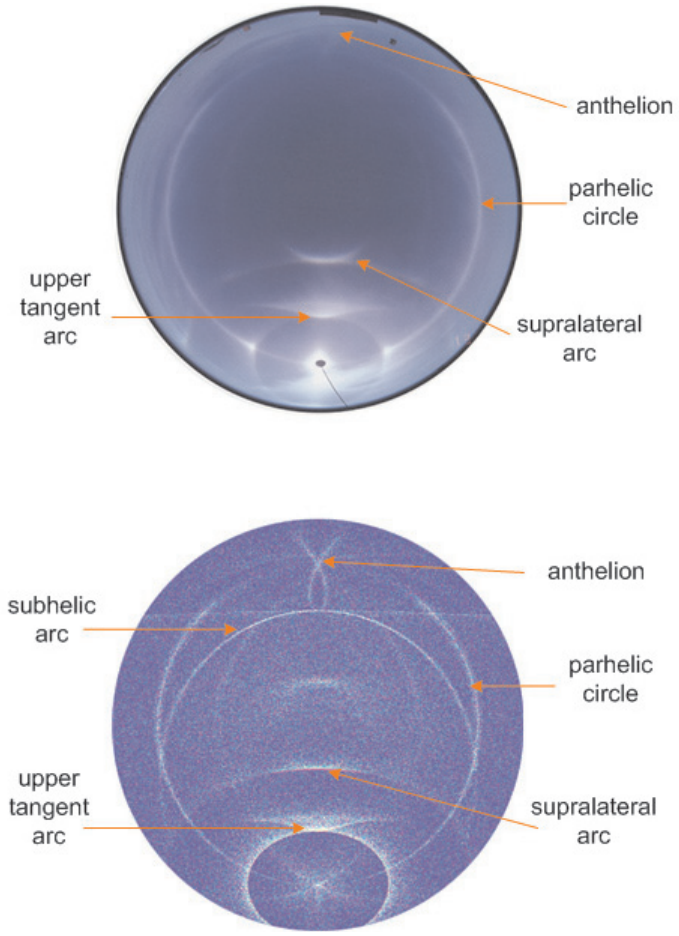

Figure 5.3: Top: Halo photo taken at the South Pole by Tape [15]; Bottom: Composite halo simulation

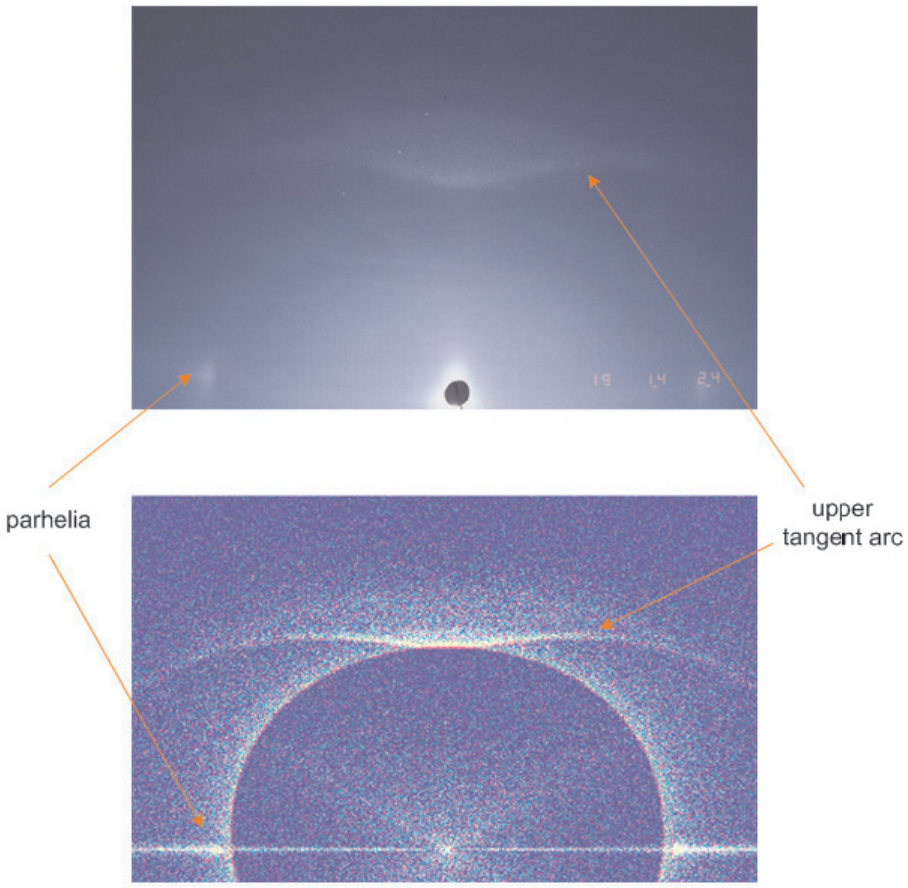

Figure 5.4: Top: upper tangent arc photo taken by Tape [15]; Bottom: upper tangent arc simulation

Chapter 6

Conclusion

In this report, the atmospheric halo phenomena have been explained and a ray tracer based on the Monte Carlo method has been presented and demonstrated. The comparison of the simulation results with the photos taken for the same phenomena shows that the ray tracer gives reasonable results. This ray tracer is very useful for simulating the phenomena and identifying atmospheric data like proportions of ice crystals and orientations. However, the halo images obtained with this ray tracer are somewhat crude, so those images are not appropriate for outdoor rendering purpose.

As briefly mentioned in chapter 3, if atmospheric rendering techniques are incorporated to the ray-tracing, then the halo images can be more physically reasonable. In addition to that, filtering methods based on non-regular sampling can improve the speckled images obtained from the inverse ray tracer. Thus future works for enhancing those roughs images without losing any physical correctness are required to adopt those techniques in the ray tracer.

References

[1] Feichtinger, H. G., Grächenig, K., and Strohmer, T. Efficient numerical methods in non-uniform sampling theory. *Numerische Mathematik 69* (1995), 423–440.

[2] Francis S. Hill, J. *Computer Graphics Using OpenGL*, second ed. Prentice Hall, Upper Saddle River, New Jersey, 2001.

[3] Gedzelman, S. D. Simulating rainbows and halos in color. *Applied Optics 33*, 21 (1994), 4607–4613.

[4] Glassner, A. Computer-generated solar halos and sun dogs. *IEEE Computer Graphics and Applications* (Mar. 1996), 77–81.

[5] Glassner, A. Solar halos and sun dogs. *IEEE Computer Graphics and Applications* (Jan. 1996), 83–87.

[6] Gonzato, J.-C., and Marchand, S. Efficient simulation of halos for computer graphics. In *8 ECS & IA*, pp. 1–6.

[7] Greenler, R. *Rainbows, halos, and glories*. Cambridge University Press, Cambridge, 1980.

[8] Hecht, E. *Optics*, third ed. Addison-Wesley, 1998.

[9] Jackèl, D., and Water, B. Simulation and visualization of halos. In *ANIGRAPH* (1998).

[10] Lynch, D. K., and Livingston, W. *Color and Light in Nature*. Cambridge University Press, Cambridge, 1995.

[11] Minneart, M. G. J. *Light and Color in the Outdoors*. Springer-Verlag, Berlin, 1993.

[12] Pattloch, F., and Tränkle, E. Monte carlo simulation and analysis of halo phenomena. *J. Opt. Soc. Am 1*, 5 (1984), 520–526.

[13] Shirley, P. *Fundamentals of Computer Graphics*. A K Peters, Natick Massachusetts, 2002.

[14] Takano, Y., and Liou, K.-N. Halo phenomena modified by multiple scattering. *J. Opt. Soc. Am 7*, 5 (1990), 885–889.

[15] Tape, W. *Atmospheric Halos*, vol. 64 of *Antarctic Research Series*. American Geophysical Union, Washington, D.C., 1994.

[16] Tränkle, E., and Greenler, R. G. Multiple-scattering effects in halo phenomena. *J. Opt. Soc. Am 4*, 3 (1987), 591–599.

Appendix A

Reflectance of Dielectrics

This appendix is extracted and summarized from [8]. If the wavelength of light is small in comparison to the size of the apparatus, one may use, as a first approximation, the techniques of Geometrical Optics. In Geometrical Optics the dominant property of light is its wave nature. Therefore as far as Geometrical Optics is concerned, it will suffice admirably to treat light as an electromagnetic wave. Suppose that the incident monochromatic lightwave is planar, so that it has the form from figure A.1

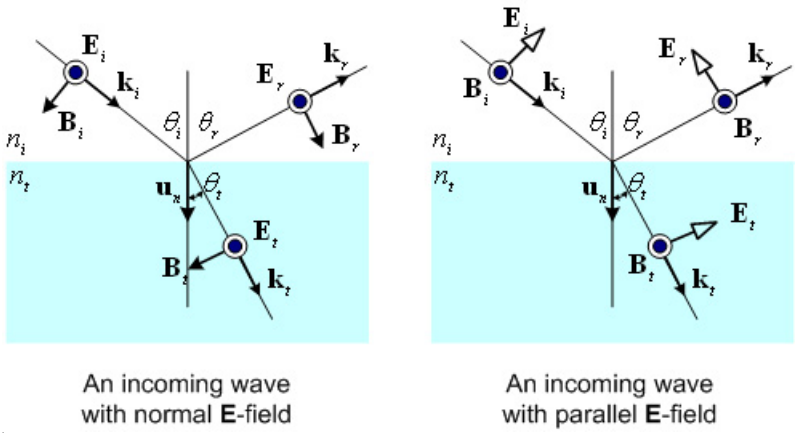

Figure A.1: Incoming waves whose **E**-fields are normal and parallel to the plane of incidence redrawn from [8].

$$\mathbf{E}_i = \mathbf{E}_{0i}\cos(\mathbf{k}_i \cdot \mathbf{r} - \omega_i t) \tag{A.1}$$
$$\mathbf{E}_r = \mathbf{E}_{0r}\cos(\mathbf{k}_r \cdot \mathbf{r} - \omega_r t + \varepsilon_r) \tag{A.2}$$
$$\mathbf{E}_t = \mathbf{E}_{0t}\cos(\mathbf{k}_t \cdot \mathbf{r} - \omega_t t + \varepsilon_t). \tag{A.3}$$

Here ε_r and ε_t are phase constants relative to $\mathbf{E}_i$ and are introduced because the position of the origin.

The laws of Electromagnetic Theory lead to certain requirements that must be met by the fields, and they are referred to as the boundary conditions. Whatever the polarization of the wave, we shall resolve its **E**- and **B**- fields into components parallel and perpendicular to the plane of incidence and treat these constituents separately. Applying the boundary condition to perpendicular and parallel **E**'s to the plane of incidence gives the following well known Fresnel Equations for dielectrics.

$$r_\perp \equiv \left(\frac{E_{0r}}{E_{0i}}\right)_\perp = \frac{n_i\cos\theta_i - n_t\cos\theta_t}{n_i\cos\theta_i + n_t\cos\theta_t} \tag{A.4}$$
$$t_\perp \equiv \left(\frac{E_{0t}}{E_{0i}}\right)_\perp = \frac{2n_i\cos\theta_i}{n_i\cos\theta_i + n_t\cos\theta_t} \tag{A.5}$$
$$r_\parallel \equiv \left(\frac{E_{0r}}{E_{0i}}\right)_\parallel = \frac{n_t\cos\theta_i - n_i\cos\theta_t}{n_i\cos\theta_t + n_t\cos\theta_i} \tag{A.6}$$
$$t_\parallel \equiv \left(\frac{E_{0t}}{E_{0i}}\right)_\parallel = \frac{2n_i\cos\theta_i}{n_i\cos\theta_t + n_t\cos\theta_i} \tag{A.7}$$

Here r denotes the amplitude reflection coefficient, and t does the amplitude transmission coefficient.

Let I_i, I_r, and I_t be the incident, reflected, and transmitted flux densities, respectively. The cross sectional areas of the incident, reflected, and transmitted beams are, respectively, $A\cos\theta_i$, $A\cos\theta_r$, and $A\cos\theta_t$. Accordingly, the incident power is $I_i A\cos\theta_i$. And similarly $I_r A\cos\theta_r$ and $I_t A\cos\theta_t$ are the reflected power and the transmitted power, respectively. We define the reflectance R to be the ratio of the reflected power to the incident power.

$$R \equiv \frac{I_r A\cos\theta_r}{I_i A\cos\theta_i} = \frac{I_r}{I_i}. \tag{A.8}$$

Similarly, the transmittance T is defined as the ratio of the transmitted to the incident flux and is given by

$$T \equiv \frac{I_t A \cos\theta_t}{I_i A \cos\theta_i}. \tag{A.9}$$

Since the quotient I_r/I_i equals E_{0r}^2/E_{0i}^2,

$$R = \left(\frac{E_{0r}}{E_{0i}}\right)^2 \tag{A.10}$$

$$T = \frac{n_t \cos\theta_t}{n_i \cos\theta_i}\left(\frac{E_{0t}}{E_{0i}}\right)^2. \tag{A.11}$$

Let's now write an expression representing the conservation of energy. The total energy flowing into area A per unit time must equal the energy flowing outward from it per unit time:

$$I_i A \cos\theta_i = I_r A \cos\theta_r + I_t A \cos\theta_t. \tag{A.12}$$

With equations A.8 and A.9, this is simply

$$R + T = 1 \tag{A.13}$$

where there was no absorption. It is convenient to use the component forms, that is,

$$R_\perp = r_\perp^2 \tag{A.14}$$

$$R_\parallel = r_\parallel^2 \tag{A.15}$$

$$T_\perp = \frac{n_t \cos\theta_t}{n_i \cos\theta_i} t_\perp^2 \tag{A.16}$$

$$T_\parallel = \frac{n_t \cos\theta_t}{n_i \cos\theta_i} t_\parallel^2. \tag{A.17}$$

Furthermore, it can be shown that

$$R_\perp + T_\perp = 1 \tag{A.18}$$

$$R_\parallel + T_\parallel = 1. \tag{A.19}$$

If the incoming light is unpolarized, we can represent it by two familiar orthogonal, incoherent, equal amplitude states. Incidentally, the fact that they are equal in amplitude means that the amount of energy in one of these two polarization states is the same as that in the other(i.e., $I_{i\parallel} = I_{i\perp} = I_i/2$). Thus,

$$I_{r\perp} = R_\perp \frac{I_i}{2} \tag{A.20}$$

$$I_{r\parallel} = R_\parallel \frac{I_i}{2}. \tag{A.21}$$

The reflectance in natural light, $R = I_r/I_i$, is therefore given by

$$R = \frac{I_{r\parallel} + I_{r\perp}}{I_i} = \frac{R_\parallel + R_\perp}{2}. \tag{A.22}$$

Index